PAPER AAS 99-161

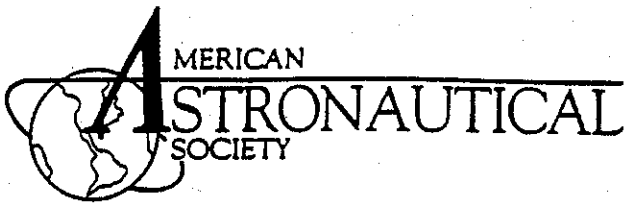

Three-Dimensional Periodic Solutions That Bifurcate From Halo Families in the Circular Restricted Three-Body Problem

K. C. Howell and E. T. Campbell

School of Aeronautics and Astronautics
Purdue University
West Lafayette, IN 47907

AAS/AIAA Space Flight Mechanics Meeting

Breckenridge, Colorado 7-10 February 1999

AAS Publications Office, P.O. Box 28130, San Diego, CA 92198

THREE-DIMENSIONAL PERIODIC SOLUTIONS THAT BIFURCATE FROM HALO FAMILIES IN THE CIRCULAR RESTRICTED THREE-BODY PROBLEM

K.C. Howell† and E.T. Campbell‡

The restricted problem of three bodies is of fundamental importance in mechanics, with significant applications to astrodynamics. During the last century, much effort has been focused on the search for periodic solutions since they are a key component in understanding the behavior in the non-integrable three-body problem. Numerous families of PLANAR periodic solutions have been computed and their relationships investigated. With vastly improved computational capabilities, THREE-DIMENSIONAL periodic families have appeared in recent years; halo orbits have, perhaps, been the most visible with their link to spacecraft mission design. Although an infinite number of three-dimensional periodic orbits exist, they are very difficult to locate, as well as compute, and a random numerical search will never be successful. Thus, the study of bifurcations, where several families come together, is critical and used as the basis of the current study. In this effort, the L_1 and L_2 halo orbits serve as the baseline families; a number of bifurcations and intersections representing the existence of other three-dimensional families are identified. Various orbits are numerically computed as members of these intersecting families. A subset of these additional periodic orbits is examined for potential mission design applications.

INTRODUCTION

The three-body problem has been the focus of much mathematical and scientific interest, and, at least, since Poincaré published his fundamental work in 1892[1], much of the serious attention has centered on the search for periodic solutions. (In fact, Poincaré considered periodic orbits the only access to understanding the behavior in the difficult three-body problem.) Early investigations quickly narrowed the study to solutions in the planar problem and a number of families of periodic orbits were identified. By 1920, some consideration was given to three-dimensional orbits; a proof of the existence of finite periodic solutions in three dimensions was offered, and some periodic orbits could be generated from certain types of infinitesimal periodic oscillations[2]. However, calculations relied heavily on analytical approximations based on assumptions concerning the structure of generating solutions near equilibrium points. Thus, it was practically impossible to determine arbitrary three-dimensional solutions. Nevertheless, there has been an enormous amount of information published on periodic solutions since the early studies[3].

† Professor, School of Aeronautics and Astronautics, Purdue University, West Lafayette, IN 47907. Email: howell@ecn.purdue.edu.

‡ Graduate Student, School of Aeronautics and Astronautics, Purdue University, West Lafayette, IN 47907. Email: ecampbel@ecn.purdue.edu.

In general, investigations concerning families of periodic orbits approach the problem in various ways: generation of families of periodic solutions from a single arbitrary orbit (both two and three dimensional); computation of three-dimensional orbits from planar solutions; definition of a "family" based on mass ratio as the parameter of interest; and, the construction of links between families by investigation of the relationships between families of planar orbits. But, many questions remain. Less emphasis has been applied to exploiting bifurcation theory to predict and compute orbits in the three-body problem. For instance, while *n*-period bifurcations have been used to predict new particular solutions in the planar problem[4,5], they have not been applied to the search for three-dimensional families of solutions. Since many of the bifurcating three-dimensional families never degenerate into planar trajectories, they may not, in fact, have been analyzed to any extent, except in a few isolated cases. To date, all three-dimensional families without at least one known planar member, can only be determined by a grid search in a three-dimensional phase space or by a systematic evaluation of three-dimensional *n*-period bifurcating solutions. In this effort, the latter method is used to determine a large number of solutions, many of which are not known to have been identified elsewhere.

One of the most intriguing aspects of the search for periodic solutions in the three-body problem is the potential for astrodynamics applications. In that context, providing more organization in the classification and "storage" of the infinite variety of periodic solutions, as well as a methodology to numerically produce a specific orbit, is clearly desirable. This cataloguing, in turn, supports mission design by offering various orbits and/or trajectory arcs as candidates in the construction of increasingly complex mission trajectories. Thus, the stability of the orbits and the flow in their vicinity become critical components in evaluating the periodic solutions. This information has, thus, been exploited in recent years. For example, the stable and unstable manifolds in the vicinity of a periodic orbit can serve as the basis for the design of transfer trajectories for arrival to and departure from periodic orbits. Gómez et al.[6], Mains[7], Barden[8], and Howell et al.[9] demonstrate three-dimensional transfers from circular parking orbits about the Earth to L_1 and L_2 halo orbits; these authors base their transfers on stable manifolds that approach the three-dimensional halo orbits. Similar techniques can be used for other missions as well[10]. Experience with both stable and unstable manifolds in the vicinity of halo families, as well as heteroclinic-type connections between such families, enabled the extension of this concept and the design of the Suess-Urey/Genesis trajectory by Howell, Barden, and Lo[11]. It is notable that some of these studies extend the computations into more complex models that include ephemeris data for the locations of bodies in the solar system; the results from the circular problem can generally be extended to these more complete dynamic models. Genesis is one very successful example. Thus, it appears that the investigation of periodic orbits as well as the flow in their vicinity and between families of such orbits will support trajectory and mission design. Ultimately, a general computational tool is sought to facilitate the design process.

As part of this larger investigation, the focus of the current effort is the search for families of periodic orbits and qualitative analysis in the restricted three-body problem; this study is undertaken with a goal toward application to trajectory design. The search is based on modern bifurcation theory that can be applied in the three-body problem and is a powerful tool for locating and relating numerically determined three-dimensional periodic solutions through stability information. It is also demonstrated that, from both the families of periodic orbits and knowledge of the flow in the vicinity of these families, transfers between the families can be constructed that are very useful in preliminary mission design. More generally, independent trajectory arcs (generated from periodic orbits or from the nearby flow) can also be "patched" together to produce nominal trajectory designs. But, the most immediate goal is the characterization of periodic orbits as well as families of periodic solutions.

BACKGROUND: CIRCULAR RESTRICTED THREE BODY PROBLEM

The Circular Restricted Three Body Problem

Given two primary bodies P_1 and P_2, arbitrarily choose mass $m_1 > m_2$. Then, in the circular restricted three body problem, differential equations governing the motion of the infinitesimal third mass P_3 are usually written in the following non-dimensional form, relative to the usual rotating coordinate frame,

$$\ddot{x} - 2\dot{y} = \frac{\partial U}{\partial x}, \qquad \ddot{y} + 2\dot{x} = \frac{\partial U}{\partial y}, \qquad \ddot{z} = \frac{\partial U}{\partial z}, \tag{1}$$

where x, y, and z are the components of the third particle relative to the system barycenter. The pseudopotential U is evaluated as

$$U = \frac{(1-\mu)}{r_1} + \frac{\mu}{r_2} + \frac{1}{2}\left(x^2 + y^2\right), \tag{2}$$

with

$$r_1 = \sqrt{(x-\mu)^2 + y^2 + z^2}, \qquad r_2 = \sqrt{(1-\mu-x)^2 + y^2 + z^2}, \tag{3}$$

and a non-dimensional mass parameter has been defined as $\mu = m_2 / (m_1 + m_2)$. The dots in equations (1) represent differentiation with respect to non-dimensional time. Equations (1) are well known to admit a constant, that is,

$$J = 2U - \left(\dot{x}^2 + \dot{y}^2 + \dot{z}^2\right), \tag{4}$$

denoted Jacobi's Integral[12]. Jacobi's constant serves to characterize families of trajectories, and it can also be used to monitor the accuracy of the numerical integration process. A number of symmetries exist in this system that aid in the search for periodic orbits. The symmetry about the xy-plane, observed in the equations of motion is of specific interest here and may eventually lead to new, independent, solutions in the problem.

Because no general solution exists for the circular restricted three-body problem, particular solutions are sought to obtain insight into the problem. Of course, the five Lagrangian points are the best known. The first three of these points, labeled L_1, L_2, and L_3, are collinear and lie on the *x*-axis. The fourth and fifth points each lie at one vertex of two equilateral triangles formed with P_1 and P_2. The collinear points are arranged such that L_1 is between P_1 and P_2, L_2 is beyond P_2, and L_3 is on the far side of the larger primary P_1. Note that the Sun-Earth-Moon system is usually modeled in the context of the circular problem by defining the primaries as the Sun and Earth/Moon barycenter (with m_1 equal to the mass of the Sun, and m_2 defined as the sum of the masses of the Earth and Moon). Appropriate libration points are then determined[13]. Of special significance, note that the linearization relative to the collinear points leads to periodic solutions that exist in the linear system. A search for such periodic solutions in the nonlinear system has been the focus of research efforts for the last 100 years.

General Periodic Orbits

The motion of a system of particles, influenced only by gravity, is defined as periodic if the position and velocity vectors associated with each particle are identical after any integer number

of fixed time intervals. In 1955, Roy and Ovenden published their well-known Periodicity Theorem to describe the motion of such a system of particles. The theorem states:

> "If *N* point-masses are moving under their mutual gravitational forces only, their orbits are periodic if, at two separate epochs, a mirror configuration occurs." *

A mirror configuration is defined in terms of an epoch, one corresponding to a state of the system such that the velocity of each of the *N* point masses in the system is perpendicular to its own radius vector, as measured from the system's stationary center of mass. Under this special condition, the Mirror Theorem of Roy and Ovenden[14] concludes that the orbit of each mass as it evolves after a mirror configuration is a mirror image of its orbit prior to the epoch corresponding to the mirror configuration. The Mirror Theorem proves that two mirror configurations are sufficient for the existence of a periodic solution. For application of the Periodicity Theorem to the circular restricted problem, it is immediately obvious that two of the three point masses, namely the two primaries, always meet the mirror configuration condition due to the fact that their states are fixed relative to the rotating coordinate frame, with velocity vectors perpendicular to position vectors. Whenever the third, infinitesimal, point mass moves on a trajectory passing through two separate mirror configurations, all three of the bodies exist in mirror configurations at two different epochs; thus, by the Periodicity Theorem, the motion of the system is periodic. Again, for the existence of a periodic orbit, it is sufficient that the trajectory of the third body includes mirror configurations at two separate epochs. To simplify the search for periodic solutions, then, initial conditions that satisfy the conditions for a single mirror configuration serve as a starting point. The state is then numerically propagated, and another mirror configuration is sought. If a second configuration can be isolated, then a periodic solution exists.

In the investigations of periodic orbits in the three-body problem, many authors, of course, have discussed symmetries and the corresponding initial state vectors[4,15-17]. In a paper published in 1980[18], Robin and Markellos state that two types of mirror configurations can occur in the circular restricted three-body problem. They denote them as (A), symmetry about an axis, and (P), symmetry about a plane. Type (A) requires the third body to cross the x-axis, the line joining the two primaries, with a velocity perpendicular to that axis. Type (P) requires the third body to cross the *xz*-plane with a velocity perpendicular to the plane. These two types of solutions are evident from the symmetry in the equations of motion as they appear in equations (1)[18]. Because two mirror configurations must occur for the existence of a symmetric periodic solution, there are actually three possible types of symmetric periodic solutions. The first type is comprised of strictly (A) configurations. It renders an orbit symmetric about the x-axis. The second type consists solely of (P) configurations and yields symmetry about the xz-plane. Both the first and second type of configurations is labeled *simply symmetric*. The third type of solution involves a mixture of (A) and (P) configurations; it produces an orbit symmetric about both the x-axis and the xz-plane. Thus, the third type is identified as a *doubly symmetric* solution. In the current work, only type (P) simply symmetric solutions are investigated.

BACKGROUND: NONLINEAR DYNAMICS

Ideally, every system of differential equations would possess an analytical solution. Both the qualitative and quantitative behavior of the system is available from an analytical solution. Unfortunately, for nearly every nonlinear system of differential equations, complete analytical solutions are not available. As an alternative, numerical simulations offer a limited view of the general system behavior. However, in the last 30 years, there has been significant progress in translating numerical information into qualitative understanding of the solution space. Dynamical systems theory is a powerful tool in the search for qualitative insight into the solution space of

* A.E. Roy and M.W. Ovenden, "On the Occurrence of Commensurable Mean Motion in the Solar System II. The Mirror Theorem," *Monthly Notes of the Royal Astronomical Society*, 1955, p. 300.

non-integrable systems such as that represented in the circular restricted three-body problem. Dynamical concepts such as bifurcations and invariant manifolds are particularly useful.

Bifurcation Theory

Bifurcation theory is the study of changes in the qualitative structure of the flow that is associated with a system of differential equations, as parameters are varied. If the flow does not change substantively for sufficiently small variations of a given parameter, the qualitative nature of the system of equations is said to be structurally stable at the given parameter value. On the other hand, if the system is not structurally stable at this parameter value, then the parameter has reached a bifurcation value, and the system of equations has evolved to a bifurcation point.

The power of bifurcation theory is the capacity to identify bifurcation points without the need for an analytical solution. For a general system of nonlinear differential equations, bifurcation points locate the qualitative transition regions along families of solutions. Furthermore, bifurcation theory enables classification of the type of transition. Before applying bifurcation theory to the circular restricted three-body problem, the relationship between the monodromy matrix and the bifurcations along families of periodic solutions must be clarified.

Monodromy Matrix, Stability, and Traditional Bifurcation Points. The monodromy matrix is the state transition matrix (also called the variational matrix) evaluated after one period along a periodic solution, i.e., $\phi(T, 0)$, where T represents the minimal period. From Floquet theory[19], stability information concerning the periodic solution can be obtained from the eigenvalues, λ_i, of the monodromy matrix. These eigenvalues are denoted as Floquet or characteristic multipliers. Three useful eigenvalue properties that apply to all monodromy matrices offer utility here. First, because the system of equations that model the circular restricted problem is Hamiltonian (Jacobi's integral is equivalent to the Hamiltonian), the system is symplectic. Further, the state transition matrix defined from any initial time to any final time is a symplectic map. All symplectic maps, including the monodromy matrix, have reciprocal eigenvalue pairs. In other words, if λ_i is an eigenvalue, then λ_i^{-1} is also an eigenvalue. Secondly, because the monodromy matrix is real, all complex eigenvalues must come in conjugate pairs, i.e., if λ_i is a complex eigenvalue, then the complex conjugate of λ_i, λ_i^*, is also an eigenvalue. Finally, because the monodromy matrix is associated with a periodic solution, there will always exist at least one unity eigenvalue; the existence of reciprocal pairs results in at least two unit eigenvalues. Of course, the determinant of the monodromy matrix is then one, and the eigenvalues are located symmetrically about the unit circle and the real axis.

The Floquet multipliers offer stability information corresponding to the periodic solution. Eigenvalues with magnitude greater (less) than one represent instability (stability). Eigenvalues on the unit circle offer no information concerning the stability of the nonlinear solution, and a higher order analysis is required. Ignoring the pair of unit eigenvalues that indicate a periodic solution, it is apparent that the linear stability of the periodic solution only depends on the four remaining eigenvalues. Because they must appear in reciprocal pairs, every stable multiplier guarantees an associated unstable eigenvalue. This fact implies that the linear instability in this system can be of order zero, one, or two. Unlike many applications, the order of linear instability yields significant information.

To correlate Floquet theory and bifurcation analysis, the concept of families of periodic solutions is introduced. Based on the definition by Goudas[15], a family of periodic solutions is a set of solutions that share a common hodograph. A hodograph is a continuous curve in phase space that consists of points belonging to different periodic solutions. In the circular restricted problem, phase space is six dimensional. However, recall that symmetric periodic solutions contain at least two mirror configurations. For example, a type (A) configuration requires that the trajectory pass through the x-axis perpendicularly. Consequently, the state vector must possess the following form: $\overline{\Psi}(t) = [\, x \;\; 0 \;\; 0 \;\; 0 \;\; \dot{y} \;\; \dot{z} \,]^{Tr}$. Similarly, a type (P) configuration dictates a state vector with the form: $\overline{\Psi}(t) = [\, x \;\; 0 \;\; z \;\; 0 \;\; \dot{y} \;\; 0 \,]^{Tr}$. In both cases, the state has only three non-zero

components. Typically, periodic solutions are determined numerically by initiating the integration at one mirror configuration and propagating the flow forward until another mirror configuration exists. Accordingly, the pair of three-dimensional hodographs associated with the two mirror configurations represents the preferred initial conditions for generation of any member of a particular family. As expected, when moving along a hodograph by varying a system parameter such as Jacobi's constant, the periodic solutions continuously evolve. In particular, the Floquet multipliers change continuously. These changes in the eigenvalues can lead to various orders of linear instability for different segments of the hodograph. A point along the hodograph at which the stability changes is a bifurcation point. There are three distinct ways that the stability can change (see Figure 1). First, a pair of eigenvalues can move along the unit circle, collide on the real axis at +1, and then continue their motion on the real axis; this behavior is denoted a tangent bifurcation. Secondly, a pair of eigenvalues can move along the unit circle and shift to the real axis at -1; such behavior indicates a period doubling bifurcation. Finally, two pairs of eigenvalues can collide on the unit circle, typically labeled a Krien collision, and split into the complex plane. This last scenario is denoted as a secondary Hopf bifurcation. Each of these bifurcations, except one specific type of tangent bifurcation called a cyclic-fold, predicts a qualitatively new periodic family, one that intersects the hodograph of the original family. The type of bifurcation dictates the qualitative differences. In this investigation thus far, the tangent and period doubling bifurcations have been exclusively studied because they both expose periodic solutions in the circular restricted three-body problem.

Bifurcations Without Order of Instability Change in the Original Solution. Unlike the traditional bifurcations discussed previously, other types occur along the original solution without a change in the order of instability. The first such type of bifurcation occurs as eigenvalues on the unit circle pass through an n^{th} root of unity, $\lambda^n = 1$ where n is an integer greater than two[20,21]. These bifurcation values aid in the location of new, qualitatively different, n-periodic solutions. The second type results from a collision of two pairs of eigenvalues on the real axis, excluding the points +1 and -1, splitting off into the complex plane. In this last case, the order of instability does not change, but the passage of the eigenvalues from real to complex values constitutes a qualitative change in the solution. This type of bifurcation will be denoted here as a modified secondary Hopf bifurcation.

Bifurcation Diagrams

A bifurcation diagram captures the relationship between bifurcating families as a system parameter is varied. In this particular problem, the parameter of choice for representing the evolution of families of periodic solutions is Jacobi's constant. A two-dimensional bifurcation diagram can be produced by plotting Jacobi's constant as a function of one of the non-zero state variables associated with a mirror configuration (i.e., the same quantities that are used to generate the hodographs). Since there are two mirror configurations along a periodic orbit, either site can be used to produce a three-dimensional hodograph and, thus, two curves result. Similarly, there are two curves on the bifurcation diagram, one associated with each hodograph, that independently represent the family. Because these particular hodographs are three-dimensional, a two-dimensional plot does imply some loss of information. For example, because two curves cross on a bifurcation diagram does not necessarily predict a hodograph intersection, that is, a bifurcation. An intersection of the curves on a bifurcation diagram is necessary but not sufficient for a bifurcation. Even so, the bifurcation diagram can make a significant contribution to an understanding of the family and its qualitative nature. As an example, consider a family of halo orbits. Halo orbits are periodic solutions in the vicinity of the collinear libration points and a representative example appears in Figure 2. Planar projections are plotted in rotating coordinates with the origin at the Earth/Moon barycenter. Note that, as expected, two mirror configurations occur along the orbit; they are labeled in the figure at the maximum z and minimum z excursion points. Since a single point, i.e., a mirror configuration, can represent the orbit, either the six-dimensional state vector at the maximum z or minimum z location would suffice. Representing each member of a family by one of these points and then collecting all such points

to define the family of orbits results in the hodograph. The halo family can be represented by either the hodograph produced by maximum z states or minimum z states. Both hodographs for the L_2 family are plotted in Figure 3 in three planar projections. The curves in Figure 4 then represent part of the corresponding bifurcation diagram for the L_2 halo family. The curve labeled "max z" is associated with the maximum z hodograph, while each point on the "min z" curve corresponds to (x, J) values associated with the minimum z excursion points for each periodic orbit of the L_2 halo family.

Along each curve in Figure 4, the solid lines indicate the family members with monodromy matrix eigenvalues that are all on the unit circle. The dashed lines, then, represent family members with a single pair of Floquet multipliers off the unit circle, i.e., one unstable eigenvalue or order-1 linear instability. The transition from one line type to another reflects a change in the order of instability; a bifurcation occurs. Note that the type of bifurcation cannot be discerned from the diagram. Beginning at the maximum x value on each curve, x is decreased until the first bifurcation occurs at the value of Jacobi's constant that corresponds to a local minimum. The bifurcation type is cyclic-fold. In general, every local extremum of the Jacobi integral, where the order of instability changes, indicates a cyclic-fold bifurcation. The phenomenon is not unique to this problem; single parameter systems generically exhibit cyclic-fold bifurcations at local extremum of the varied parameter[19,22]. Cyclic-fold bifurcations can occur at other locations in this problem as well, since there is no evidence to suggest that this is merely a single parameter system. Continuing along the curves, the next two bifurcations are period doubling, denoted $2P_{2c}$ and $2P_{2d}$. (The designation $2P_{2c}$, for example, indicates the third (subscript c) 2-period solution (2P) computed from the original L_2 halo family (subscript 2).)

Stability Diagrams

In contrast to a bifurcation diagram, a stability diagram can be used to identify the type of bifurcation that occurs along the hodograph. Such a stability diagram is used by Broucke[23] in the circular restricted three-body problem dating from 1969 and later generalized by Howard and Mackay[24] in 1987. Because the monodromy matrix is real and symplectic, the associated characteristic equation has the following form

$$P(\lambda) = \lambda^4 - A\lambda^3 + B\lambda^2 - A\lambda^1 + 1, \tag{5}$$

where A and B are real coefficients, and the pair of eigenvalues at +1 have been factored out since they offer no stability information. Using equation (5), it is simple to solve $P(\lambda) = 0$ for λ = +1 and −1. These two critical points lead to two possible linear relationships between the coefficients A and B, namely,

$$B = 2A - 2, \tag{6}$$

and

$$B = -2A - 2, \tag{7}$$

respectively. The linear equations (6) and (7) represent the locus of potential tangent and period doubling bifurcation points, respectively. For the set of all possible collisions resulting in complex eigenvalues off the unit circle, a quadratic relationship exists, that is,

$$B = A^2/4 + 2. \tag{8}$$

When $-4 < A < 4$, equation (8) represents the locus of secondary Hopf bifurcations. For $-\infty < A < -4$ and $4 < A < \infty$, the quadratic equation is the set of all possible modified secondary Hopf bifurcations. Plotting B versus A for each point on a hodograph, along with equations (6) - (8), yields a stability diagram (where the dotted lines in Figure 5 represent the relationships in equations (6) – (8)). Notice that the only region that has order-0 instability encloses the origin. The upper boundary of this area is defined by equation (8), evaluated between A = –4 and 4. This fact establishes the range of A over which secondary Hopf bifurcations are possible, since they involve eigenvalues leaving the unit circle for the complex plane. Note, equations (6) and (8) are simultaneously satisfied at A = 4 while equations (7) and (8) intersect at A = –4. The crossings of the quadratic Hopf line with both the tangent and period doubling lines at A = +4 and A = –4, respectively, explains their exclusion from the locus of secondary Hopf bifurcations; secondary Hopf bifurcations occur away from the Floquet multiplier values of ±1.

The locus of *n*-period bifurcations, for *n* = 3, 4, ..., can be computed relatively simply[5] by solving $P(\lambda) = 0$, where λ is the subset of $\lambda^n = 1$ that excludes the solutions $\lambda^j = 1$ for *j* = 1, 2, ..., $n-1$. For example, let *n* = 3. The three roots of unity are +1, $e^{2\pi i/3}$, $e^{4\pi i/3}$. But, +1 is also a root of unity for *n* = 1, thus λ is the set composed of $e^{2\pi i/3}$ and $e^{4\pi i/3}$. Substitution of these two values into $P(\lambda) = 0$ yields the linear coefficient relationship

$$B = -A + 1. \tag{9}$$

Similarly, for *n* = 4, the relationship becomes

$$B = 2, \tag{10}$$

for $\lambda = e^{\pi i/4}$ and $e^{3\pi i/4}$. When *n* = 5, two unique linear equations are produced, i.e.,

$$B = \left(\frac{-0.5}{\cos\frac{4\pi}{5}} \right) A - \left(\frac{\cos\frac{8\pi}{5} + 1}{\cos\frac{4\pi}{5}} \right), \tag{11}$$

for $\lambda = e^{2\pi i/5}$ and $e^{8\pi i/5}$, and

$$B = \left(\frac{-0.5}{\cos\frac{8\pi}{5}} \right) A - \left(\frac{\cos\frac{16\pi}{5} + 1}{\cos\frac{8\pi}{5}} \right), \tag{12}$$

for $\lambda = e^{4\pi i/5}$ and $e^{6\pi i/5}$. Of course, this process could be continued indefinitely for all *n*, but $n \leq 5$ is sufficient to demonstrate identification of *n*-periodic bifurcations along a family. These additional relationships also appear in the region near the origin in the stability diagram in Figure 5. Again, by overlaying B as a function of A for each point on a hodograph, along with equations (6) through (12), *n*-periodic bifurcations can be identified for *n* = 1, 2, ..., 5. (Note, 1-period

represents a tangent bifurcation. This is consistent with the fact that if a new solution exists, tangent bifurcations do not alter the period.)

RESULTS

The work completed thus far in this investigation applies bifurcation theory to the three-dimensional circular restricted three-body problem. Over 30 families have been mapped and their stability recorded. Many of these families are generated systematically using bifurcation theory. The L_2 halo family is discussed here as a demonstrative example. Thus far, there are 12 families of solutions that are known to bifurcate from the L_2 family. In this section, only the four 2-period and three 3-period bifurcating families will be presented.

Halo Families

It is fortunate that analytical approximations are now available[25-27] for some halo orbits, under certain conditions. These approximations yield two important capabilities. First, a higher order approximation supplies the critical first guess for a numerical corrections process that will subsequently converge to a periodic orbit. This capability is, in turn, a key component for mapping an entire family. Secondly, the mapping can be checked for validity over the portion of the hodograph near the Lagrangian point. Families of periodic orbits have been determined that bifurcate from both L_1 and L_2 halo families. The following section describes some of the results obtained for the L_2 halo family.

L_2 Halo Family. Using a 25^{th} order polynomial approximation and an out-of-plane z value of 10^{-5} meters relative to the L_2 equilibrium point, an initial L_2 halo is numerically determined by applying a differential corrections process. Beginning with this family member, a large section of the family is subsequently mapped out. Recall that the planar projections of the associated minimum and maximum z mirror configuration hodographs for the northern L_2 family can be seen in Figure 3. Following the hodographs toward the Earth/Moon barycenter, both the maximum and minimum z mirror configurations approach the singularity. (In the xz-projection, the large, positive out-of-plane z amplitude peaks at approximately 1,900,000 km and decreases toward zero as x decreases; the z amplitude below the plane also returns to zero near the Earth/Moon barycenter.) The family is tracked until its closest approach to the Earth/Moon barycenter is 5 km. Because of the relatively large $\dot{y}$ values obtained near the singularity and the consequent scaling of all other curves to straight lines, orbits with a closest approach of 2284 km or smaller are not included in Figure 3. Again, these are northern hodographs. Planar projections of southern hodograph projections are mirror images across the xy-plane. Henceforth, without loss of generality, only northern L_2 orbits and their bifurcating solutions are discussed.

The bifurcation diagram that includes all of the L_2 data can be found in Figure 6. Following the curves from the maximum x value (near the L_2 point) inward toward the origin, the family is initially order-1 unstable. The first bifurcation, yielding the $2P_{2a}$ family, is period doubling, which increases the instability order to 2. Shortly thereafter, another period doubling occurs, generating the $2P_{2b}$ family, returning the family to order-1 instability. Next, a cyclic-fold bifurcation occurs at the local minimum of Jacobi's constant. Now the family has order-0 instability. Then a 2-period bifurcation, spawning the $2P_{2c}$ family, brings the system back to order-1 instability. The last stability change occurs close to the Earth/Moon barycenter when all of the eigenvalues return to the unit circle and is period doubling, yielding the $2P_{2d}$ family.

A more thorough analysis of the possible bifurcations to new families of solutions can be seen in the modified stability diagram, Figure 7. This L_2 stability diagram shows many *n*-period bifurcations as well as the stability changes already apparent from Figure 6. The point on the solid curve at the largest A and B values corresponds to the family member with the largest x value (also, it is the closest member to the L_2 equilibrium solution) as seen in Figure 3 and Figure 6. As the family, represented by the solid line in Figure 7, evolves toward the Earth/Moon singularity, it undergoes the following bifurcations: a 5-period (family $5P_{2a}$), 4-period (family $4P_{2a}$),

3-period (family $3P_{2a}$), 5-period (family $5P_{2b}$), and two 2-period (families $2P_{2a}$ and $2P_{2b}$). A zoom view of the origin in Figure 7 is plotted in Figure 8. Continuing along the solid curve from the lower right, the following bifurcations occur: a 5-period (family $5P_{2c}$), tangent (cyclic-fold), two 5-period, a 2-period (family $2P_{2c}$), 5-period, 2-period (family $2P_{2d}$), 5-period, 4-period (family $4P_{2b}$), 3-period (family $3P_{2b}$), and a 5-period. The various properties and characteristics of each of the 2- and 3-period L_2 halo bifurcating solutions are discussed below.

2-Period Bifurcating Solutions. All four of the 2-period families that result from bifurcations have been determined. Members of these families are type (P) simply symmetric. The four families have been denoted $2P_{2a}$, $2P_{2b}$, $2P_{2c}$, and $2P_{2d}$. The planar projections of the family hodographs, along with the associated section of the L_2 halo minimum and maximum z mirror configuration hodographs appear in Figure 9. Notice that each 2-period family is apparently represented solely by a single continuous hodograph, one that only intersects with one of the two L_2 halo hodographs in three-dimensional phase space. The location at which the intersection occurs, whether on the max z or min z L_2 hodograph, identifies the new solution as a result of bifurcating exclusively from the maximum z or minimum z mirror configuration. The $2P_{2a}$ and $2P_{2d}$ families originate from the L_2 maximum z hodograph, while $2P_{2b}$ and $2P_{2c}$ families depart from the minimum z configuration hodograph. The $2P_{2a}$ and $2P_{2d}$ families are defined as northern, since their state vectors at the mirror configurations have positive z components. Likewise, the $2P_{2b}$ and $2P_{2c}$ families are labeled southern. Of course, it is important to realize that all four 2-period families do actually include both northern and southern solutions. The particular type of solution that is identified here to represent these period doubling families results strictly from bifurcations off of the northern L_2 halo family. The planar projections of a typical southern 2-period solution, in this case a $2P_{2c}$ family member, is featured in Figure 10. First, observe in the figure that points labeled A and B identify the max z and min z points along the L_2 halo orbit. Then, it is apparent that the $2P_{2c}$ family member has two local minimum z mirror configurations (C and D) that develop from the single northern L_2 minimum z mirror configuration state (A). Graphically, the mirror configuration at point A on the halo orbit splits into points C and D on the $2P_{2c}$ family, while the mirror configuration at point B on the halo does not have a corresponding point in the $2P_{2c}$ family. Points C and D represent two local minimum z mirror configurations. Note that point C in the 2-period family passes closer to the Earth/Moon primary than the corresponding point A along the halo orbit. This splitting of the L_2 halo minimum z mirror configuration point affords two mirror configuration hodographs for the 2-period solution, as expected for a symmetric periodic solution. But, these hodographs are joined at the bifurcating L_2 minimum z point. Consequently, in Figure 9, a different $2P_{2c}$ curve lies to each side of the L_2 "min z" hodograph; the two hodographs join at the intersection with the L_2 family, and together they appear as a single continuous line. The bifurcation diagram of the four families, plus the appropriate portion of the L_2 family, appears in Figure 11. Notice that each 2-period family, at the period doubling bifurcation point, has a local extremum in Jacobi's constant. Further, the new families do not have a stability change at this point; however, the stability of the orbits along the original L_2 halo family does change as the family hodograph passes through the bifurcation point. The numerous bifurcations and stability changes within these new families have yet to be fully investigated.

3-Period Bifurcating Solutions. Both 3-period families of periodic orbits that bifurcate from the L_2 halo family, $3P_{2a}$ and $3P_{2b}$, have been partially mapped. Each member of a 3-period family is type (P) simply symmetric with mirror configurations denoted as being either associated with a local maximum or minimum excursion point in z. In Figure 12, a typical northern 3-period solution and the associated bifurcating L_2 family member is plotted. Here, the designation "northern" implies that this 3-period solution originates from a northern L_2 halo. Careful observation of the figure reveals two mirror configurations along the orbit. Because these two mirror configurations along the 3-period orbit do not collapse into a single configuration, as in the 2-period case, there will be two noncontiguous hodographs associated with each 3-period family. These hodographs intersect the two L_2 halo hodographs simultaneously (see Figure 13). The $3P_{2b}$ family does not appear in this figure since it resides very close to the Earth/Moon singularity. The $\dot{y}$ values

corresponding to the $3P_{2b}$ family, near the bifurcation point, range from 40 km/s to 200 km/s. These values completely eclipse the $3P_{2a}$ values, and are consequently left out of Figure 13. Since 3-period bifurcations, along with all *n*-period bifurcations, for $n > 2$, are pitchfork in nature (though no stability change occurs at the common bifurcation point of either family), both the minimum and maximum mirror configuration along the 3-period family will be at a local extremum of Jacobi's Integral. This fact can be seen in Figure 14, the bifurcation diagram. Again, this fact will be true for all odd-periodic solutions. In this case, at this resolution, the minimum $3P_{2b}$ mirror configuration hodograph appears overlaid with the minimum excursion L_2 hodograph. At higher resolutions, it is clear that the two curves are distinct. Further, the $3P_{2b}$ minimum z hodograph is at an extremum in Jacobi's constant as it crosses the minimum L_2 mirror configuration hodograph. Additional stability and bifurcation analysis of the 3-period families has not yet been completed.

Connections between Different Families

Besides the 2-period and 3-period families discussed in the preceding section, numerous other families have also been generated, including some 4-period and 5-period orbits. However, beyond generating a large number of families of solutions, it is of fundamental importance to understand how these families are related. The families might intersect in configuration space. They could also have intersecting stable and unstable manifold surfaces. Such conditions offer an opportunity to shift between particular solutions, i.e., between different families of periodic orbits or transfer from one specific orbit to another. Below, two examples are discussed to demonstrate the concept.

Intersections of Families. In shifting from one family (or orbit) to another, a change in velocity, $\Delta\overline{V}$, is generally required. The three planar projections of the maximum and minimum type (P) hodographs for the northern and southern L_1 and L_2 halo families, as well as the hodographs for two additional families, labeled Poisson-1 and Poisson-2, appear in Figure 15. Note that the orbits in the two Poisson families represent independent families of periodic orbits. These families have appeared in other studies and the families can be mapped out after a single member is identified. The hodographs representing the Poisson families obviously cross the halo family hodographs, however, these crossings do not represent bifurcations. Returning to Figure 15, observe the halo and Poisson hodograph intersections. At every line crossing in the xz plot, a velocity shift in the $\hat{y}$ direction can be implemented to "jump" between the two families. For instance, the asterisks in Figure 15 represent the spatial intersection of a northern and southern L_1 halo with a Poisson-1 family member at its type (P) mirror configurations. The actual family members appear in Figure 16. For an astrodynamics application, assume a vehicle is originally moving in the northern L_1 halo and consider a transfer into the southern L_1 halo. A velocity discontinuity exists, and a 114 m/s $\Delta\overline{V}$ executed in the $\hat{y}$ direction at the minimum z type (P) mirror configuration will immediately shift the vehicle into the Poisson-1 orbit at its minimum z type (P) mirror configuration. One half period later, at the Poisson-1 maximum z type (P) mirror configuration, implementation of another 114 m/s maneuver in the negative $\hat{y}$ direction will result in a shift into the southern L_1 halo. The southern orbit is exactly the same size as the original northern L_1 halo. Thus a transfer from a northern to a southern L_1 halo is accomplished at a total cost of 228 m/s. These transfers demonstrate possible ways that different families are related. Further understanding of the connection between families may lead to a systematic methodology to locate seemingly unrelated families and/or serve as a basis for the construction of complex trajectories to meet specific objectives.

An extended technique for transfers between families also exists. Namely, after numerically approximating many families, it is possible to discern where, if at all, families intersect in three-dimensional configuration space. At these lines of intersection, a single maneuver can complete a shift from one orbit or family to another. In this way, examining sets of intersecting surfaces is the first step necessary to develop a new approach for preliminary mission design in the circular restricted three-body problem.

Stable and Unstable Manifold Transfers. Another method of transferring between families involves the intersection of stable and unstable manifolds associated with periodic orbits. If an unstable manifold from a generic periodic solution, Orbit #1, should spatially intersect the stable manifold of another periodic solution, Orbit #2, then a shift from one orbit to another is possible with a jump in velocity. One example, plotted in Figure 17, is a transfer from a northern L_1 halo to a southern L_2 halo, one that can be accomplished with a single $\Delta\vec{V}$ of magnitude 2.39 m/s and a flight time of approximately 110 days. Note that there are an infinite number of such manifold crossings between the L_1 and L_2 halo families, each offering a single maneuver to complete such a transfer. The result that appears in Figure 17 offers both a reasonable cost and transfer time. (It can also be extended into a model that includes solar radiation pressure as well as ephemeris data for the location of the planets. The concept demonstrated in Figure 17 is, of course, exploited very successfully in the design of the Genesis trajectory[11].) Another example, one that appears in Figure 18, involves a transfer from a $2P_{1a}$ orbit to a $2P_{2a}$ solution for a modest $\Delta\vec{V}$ of magnitude 1.19 m/s and a 270 day transfer time. With the Earth/Moon barycenter at the origin, the path extends from the vicinity of L_1 as far as the distance of L_2 on the far side of the primary. The final example, a $3P_{1a}$ to a $3P_{2a}$ transfer, illustrates a potential trajectory design option with an objective function that minimizes the $\Delta\vec{V}$ cost while releasing the time of flight constraint. The two 3-period periodic orbits appear in Figure 19; the Earth/Moon barycenter is located at the origin and the equilibrium points are then also marked in the x-axis. Note that these periodic orbits are members of families that bifurcate from the L_1 and L_2 halo families, respectively. The result appears in Figure 20, that is, the $3P_{1a}$ periodic orbit, the corresponding unstable manifold, the maneuver point (marked with the symbol "+"), the stable manifold of the target orbit and, finally, the final $3P_{2a}$ periodic orbit. In this case, the cost is 9.05 m/s with a transfer time of approximately 500 days. It is notable that the result is obtained automatically once the families of periodic orbits are mapped; the stable and unstable manifolds are then automatically computed and intersections sought. The complexity of the solution is evidence that such a result could not be generated from a trial and error process. Although this particular result may not be currently applicable, it demonstrates the methodology and development of this strategy is continuing. In general, spatial manifold intersections occur between all unstable families. Exploring these types of transfers reveals ultimately practical strategies for shifting between orbits in different families of periodic solutions.

CONCLUDING REMARKS

Combining these techniques, such concepts can be useful for mission design if the results can be exploited to link together various three-body trajectory arcs. While the three-body model more accurately represents significant regions in the solar system, it is exceedingly more challenging to locate desirable trajectories. However, the knowledge gained from a large library of known families of solutions and a better understanding of the relationships between families, as well as their stability characteristics, offers access to manifold (stable, unstable and center) information which may greatly simplify this inherently difficulty task.

ACKNOWLEDGEMENTS

The authors are indebted to G. Gómez, J. Masdemont, and C. Simó for some supporting software. It is also noted that portions of this work were supported by Purdue University.

REFERENCES

1. H. Poincaré, *Les Méthodes Nouvelles de la Mécanique Céleste,* Vol. 1, 1892; *New Methods of Celestial Mechanics, (English Translation)*, Vol. 13, History of Modern Physics and Astronomy, American Institute of Physics, 1993.

2. F.R. Moulton, *Periodic Orbits*, Carnegie Institution of Washington Publications, No. 161, Washington, 1920.

3. K.C. Howell, "Families of Orbits in the Vicinity of the Collinear Libration Points," Paper No. 98-4465, AIAA/AAS Astrodynamics Specialist Conference, Boston, Massachusetts, August 1998.

4. M. Hénon, *Generating Families in the Restricted Three-Body Problem,* Springer-Verlag, New York, 1997.

5. G. Iooss, and D. Joseph, "Bifurcation and Stability of nT-Periodic Solutions Branching from T-Periodic Solutions at Points of Resonance," *Archive for Rational Mechanics and Analysis*, Vol. 66, 1977.

6. G. Gómez, A. Jorba, J. Masdemont, and C. Simó, "Study of the Transfer from the Earth to a Halo Orbit Around the Equilibrium Point L_1," *Celestial Mechanics and Dynamical Astronomy,* Vol. 56, No. 4, 1993, pp. 541-562.

7. D. Mains, "Transfer Trajectories from Earth Parking Orbits to L1 Halo Orbits," M.S. Thesis, Purdue University, West Lafayette, Indiana, 1993.

8. B.T. Barden, "Using Stable Manifolds to Generate Transfers in the Circular Restricted Problem of Three Bodies," M.S. Thesis, School of Aeronautics and Astronautics, Purdue University, West Lafayette, Indiana, 1994.

9. K.C. Howell, D.L. Mains, and B.T. Barden, "Transfer Trajectories from Earth Parking Orbits to Sun-Earth Halo Orbits," *AAS/AIAA Space Flight Mechanics Meeting 1994,* Advances in the Astronautical Sciences, Vol. 87, J. Cochran, C. Edwards, S. Hoffman, and R. Holdaway (editors), 1994, pp. 399-422.

10. J.J. Guzmán, D.S. Cooley, K.C. Howell, and D. Folta, "Trajectory Design Strategies for Libration Point Missions that Incorporate Invariant Manifolds and SWINGBY," Paper No. AAS 98-349, AAS/GSFC International Symposium on Space Flight Dynamics, Greenbelt, Maryland, May 1998.

11. K.C Howell, B. T. Barden, and M. W. Lo, "Application of Dynamical Systems Theory to Trajectory Design for a Libration Point Mission," *Journal of the Astronautical Sciences*, Vol. 45, No. 2, 1997, p. 161 - 178.

12. V. Szebehely, *Theory of Orbits*, Academic Press, New York, 1967.

13. R.W. Farquhar, "The Moon's Influence on the Location of the Sun-Earth Exterior Libration Point," *Celestial Mechanics*, Vol. 2, 1970, p. 131 - 133.

14. A.E. Roy and M.W. Ovenden, "On the Occurrence of Commensurable Mean Motion in the Solar System II. The Mirror Theorem," *Monthly Notes of the Royal Astronomical Society*, 1955, p. 300.

15. C.L. Goudas, "Three-Dimensional Periodic Orbits and Their Stability," *Icarus,* Vol. 2, 1963, p. 1-18.

16. M. Hénon and M. Guyot, "Stability of Periodic Orbits in the Restricted Problem," *Periodic Orbits, Stability, and Resonances,* D. Reidel Publishing Company, Dordrecht-Holland, 1970, p. 349-374.

17. R. Broucke and D. Boggs, "Periodic Orbits in the Planar General Three-Body Problem," *Celestial Mechanics,* Vol. 11, 1975, p.13-38.

18. I.A. Robin and V. V. Markellos, "Numerical Determination of Three-Dimensional Periodic Orbits Generated From Vertical Self-Resonant Satellite Orbits," *Celestial Mechanics*, Vol. 21, 1980, p. 395 - 434.

19. A.H. Nayfeh and B. Balachandran, *Applied Nonlinear Dynamics \ Analytical, Computational, and Experimental Methods*, John Wiley & Sons, Inc., New York, 1995, p. 205.

20. L.E. Reichl, *The Transition to Chaos \ In Conservative Classical Systems: Quantum Manifestations*, Springer-Verlag, New York, 1992, p. 114.

21. Y.A. Kuznetsov, *Elements of Applied Bifurcation Theory*, Springer-Verlag, New York, 1995.

22. J. Hale and H. Koçak, *Dynamics and Bifurcations*, Springer-Verlag, New York, 1996, p. 514.

23. R. Broucke, "Stability of Periodic Orbits in the Elliptic, Restricted Three-Body Problem," *AIAA Journal*, Vol. 7, No. 6, June 1969.

24. J.E. Howard and R. S. MacKay, "Linear Stability of Symplectic Maps", *Journal Math. Phys.*, Vol. 28, No. 5, May 1987.

25. D.L. Richardson, "Analytic Construction of Periodic Orbits About the Collinear Points," *Celestial Mechanics*, Vol. 22, 1980, p. 241 - 253.

26. C. Simó, A. Jorba, J. Masdemont, and G. Gómez, "Final Report: Study Refinement of Semi-Analytical Halo Orbit Theory," ESOC Contract Report, Technical Report, April 1991.

27. L. Carpenter, "Periodic Orbits in Trigonometric Series," *Periodic Orbits, Stability and Resonances*, D. Reidel Publishing Company, Dordrecht-Holland, 1970, p. 192 - 208.

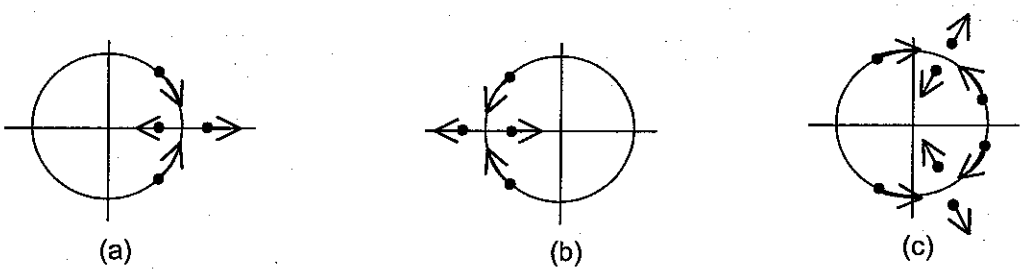

Figure 1 (a) Bifurcation at +1, +1, (b) Bifurcation at −1, −1, and (c) Bifurcation on Unit Circle.

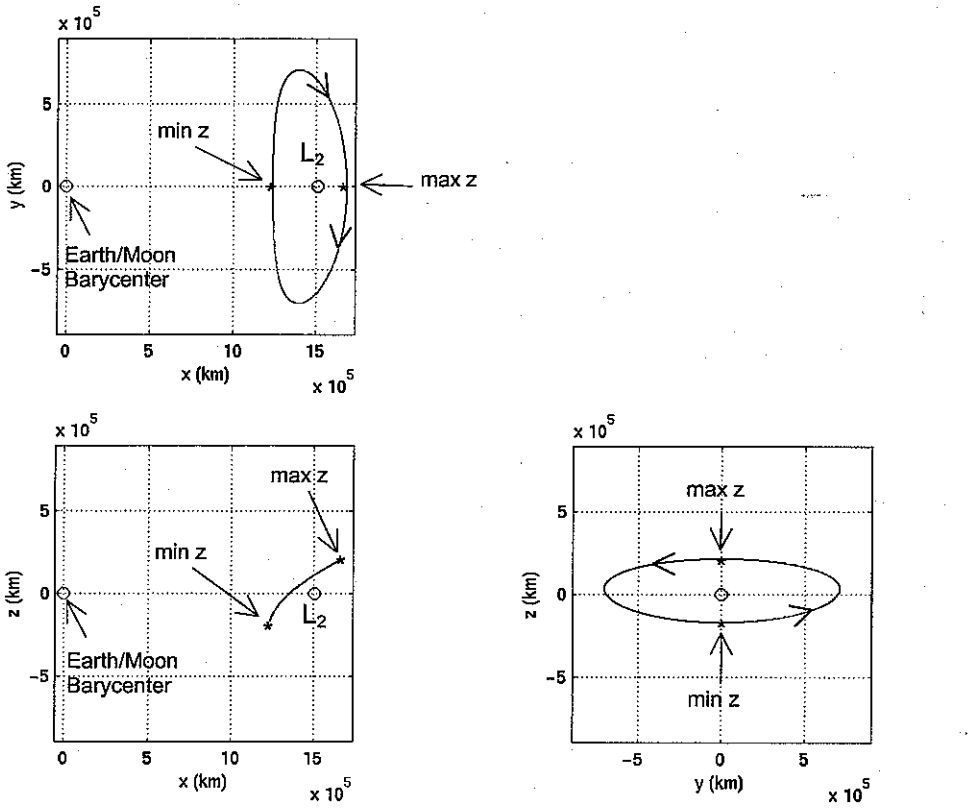

Figure 2 An L_2 halo with both the maximum and minimum z mirror configurations labeled.

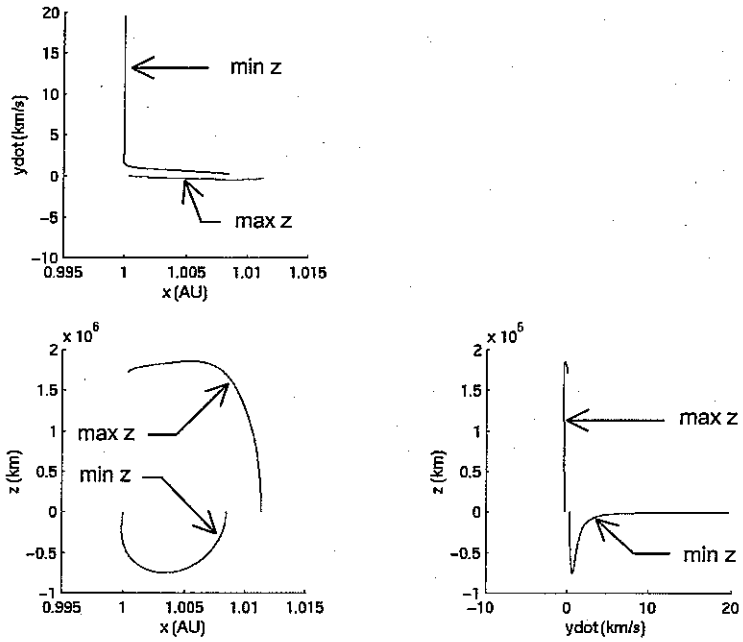

Figure 3 Three planar projections of the northern L_2 halo hodographs.

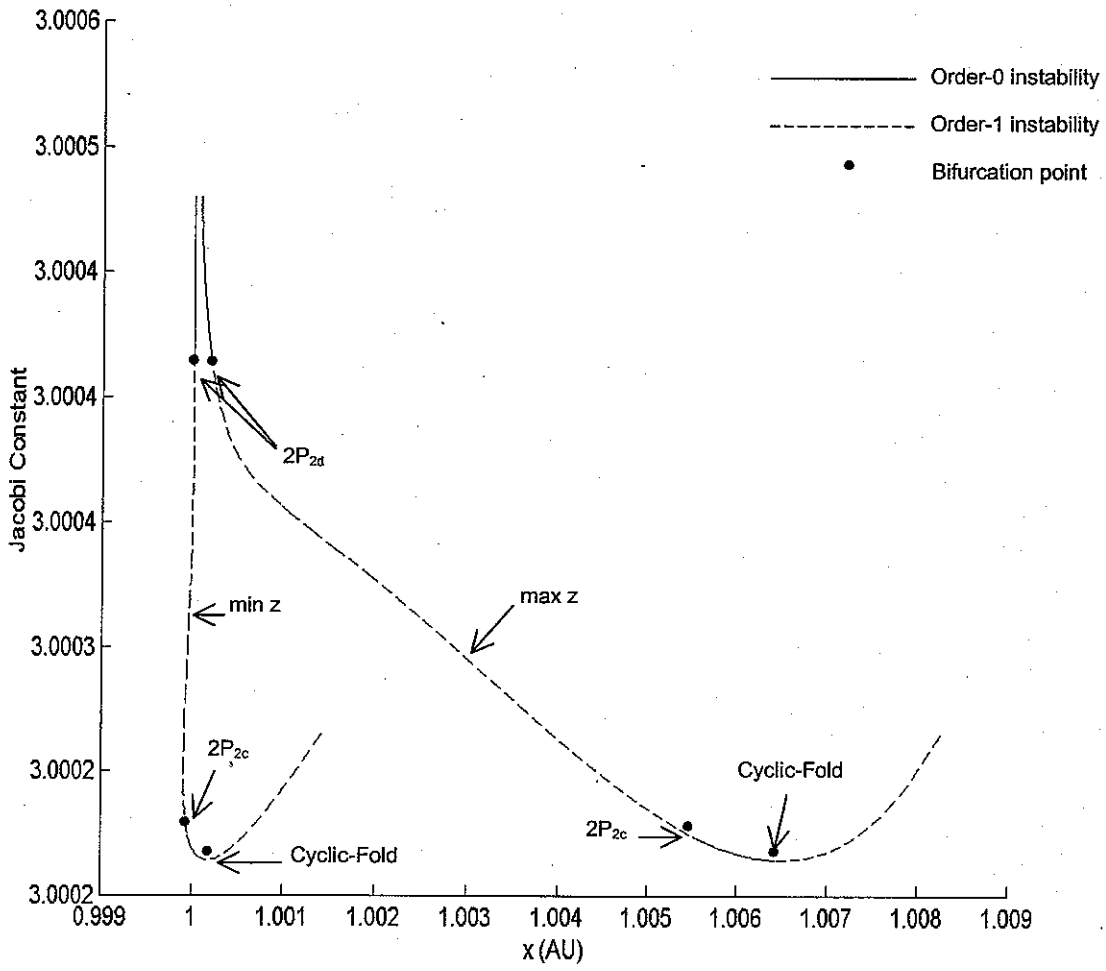

Figure 4 Northern L_2 halo bifurcation diagram

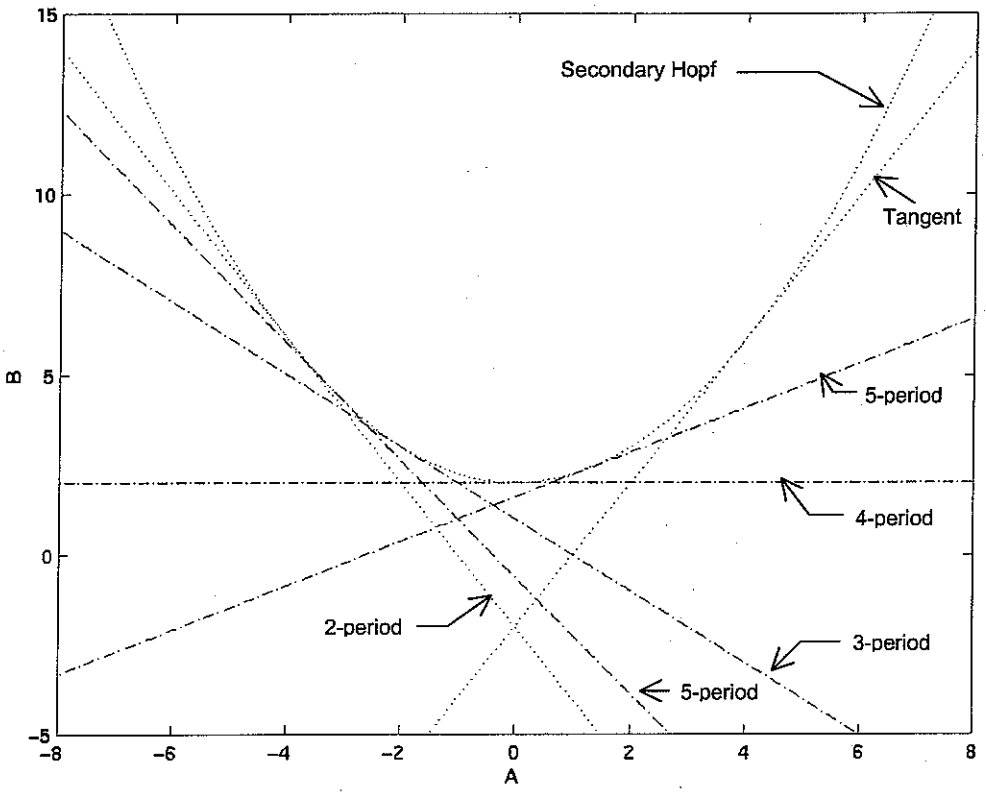

Figure 5 Generic *n*-period stability diagram for $n = 1, \ldots, 5$.

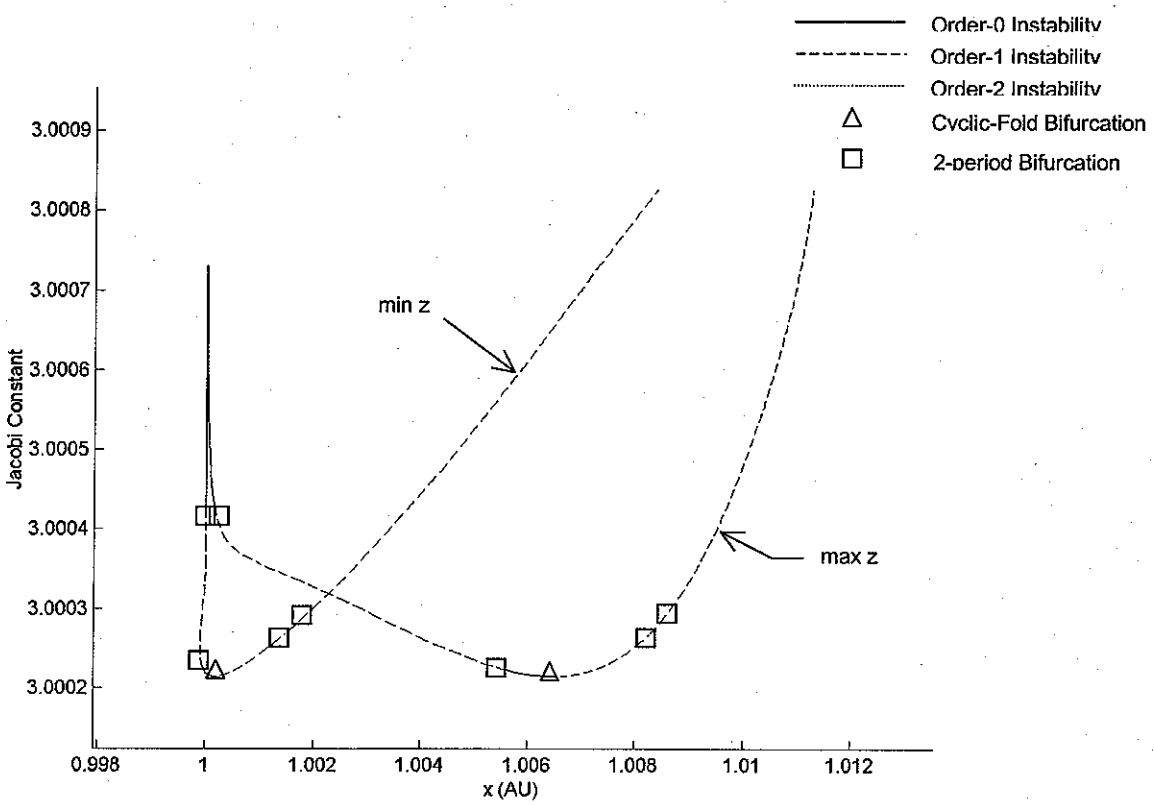

Figure 6 L_2 halo bifurcation diagram.

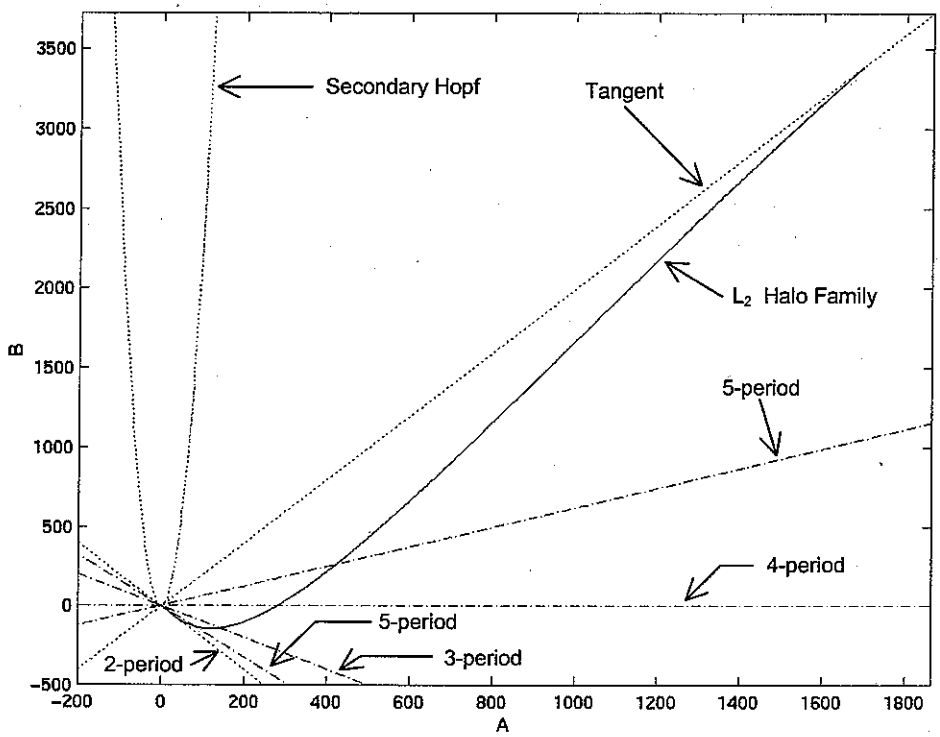

Figure 7 L_2 halo stability diagram.

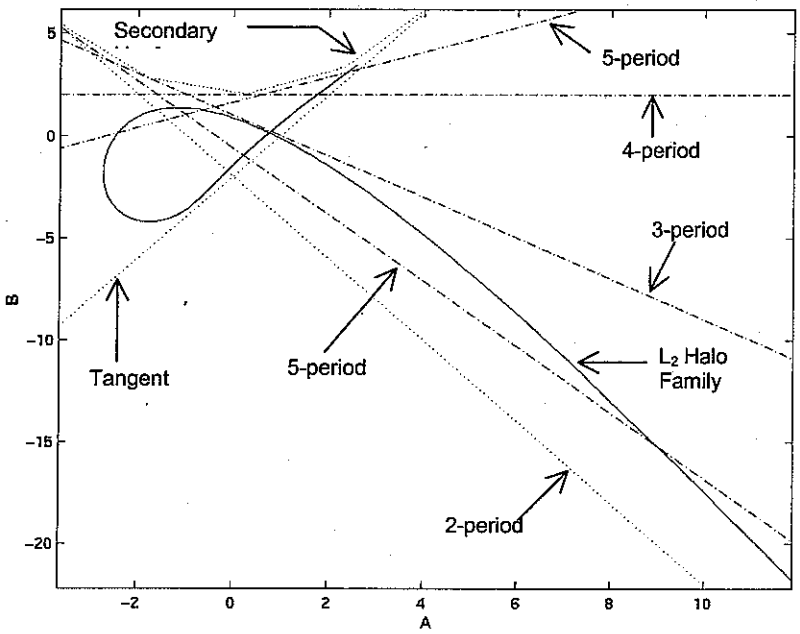

Figure 8 Close up view of the origin of Figure 7.

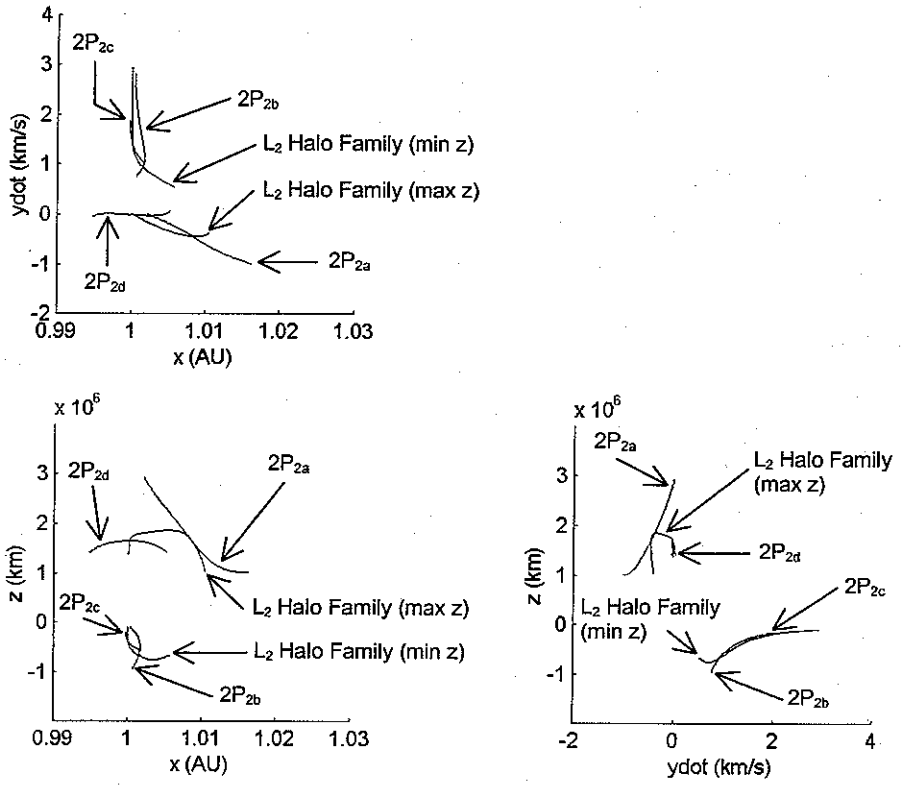

Figure 9 Northern hodographs: planar projections of the L_2 halo, $2P_{2a}$,, $2P_{2b}$, $2P_{2c}$, and $2P_{2d}$ families.

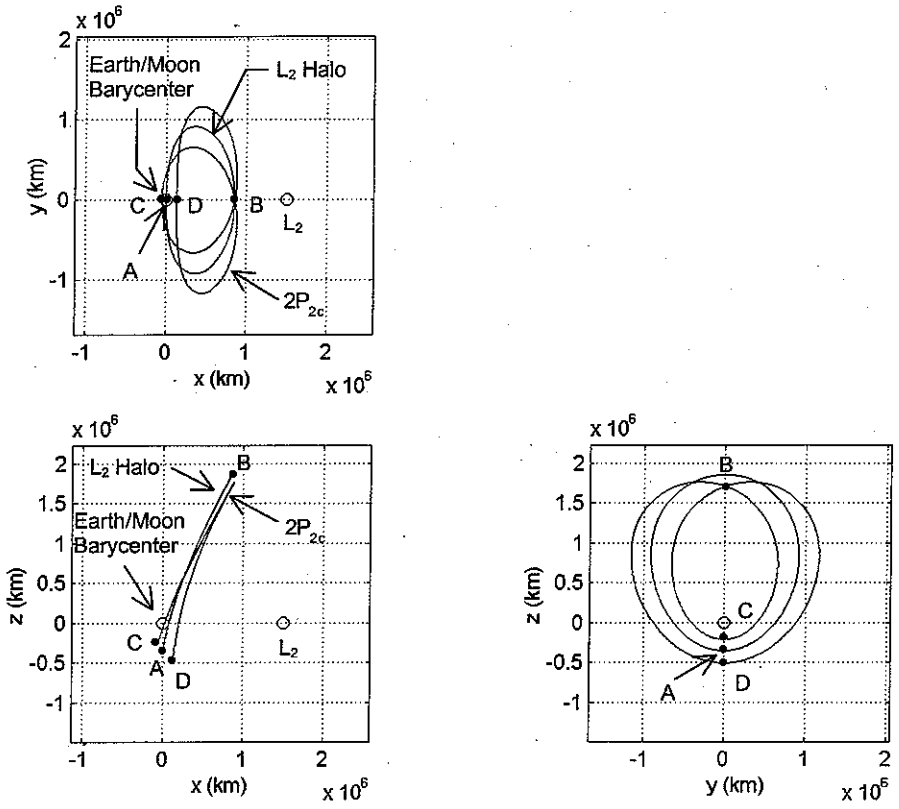

Figure 10 A $2P_{2c}$ minimum z mirror configuration bifurcation orbit and the associated bifurcating L_2 halo.

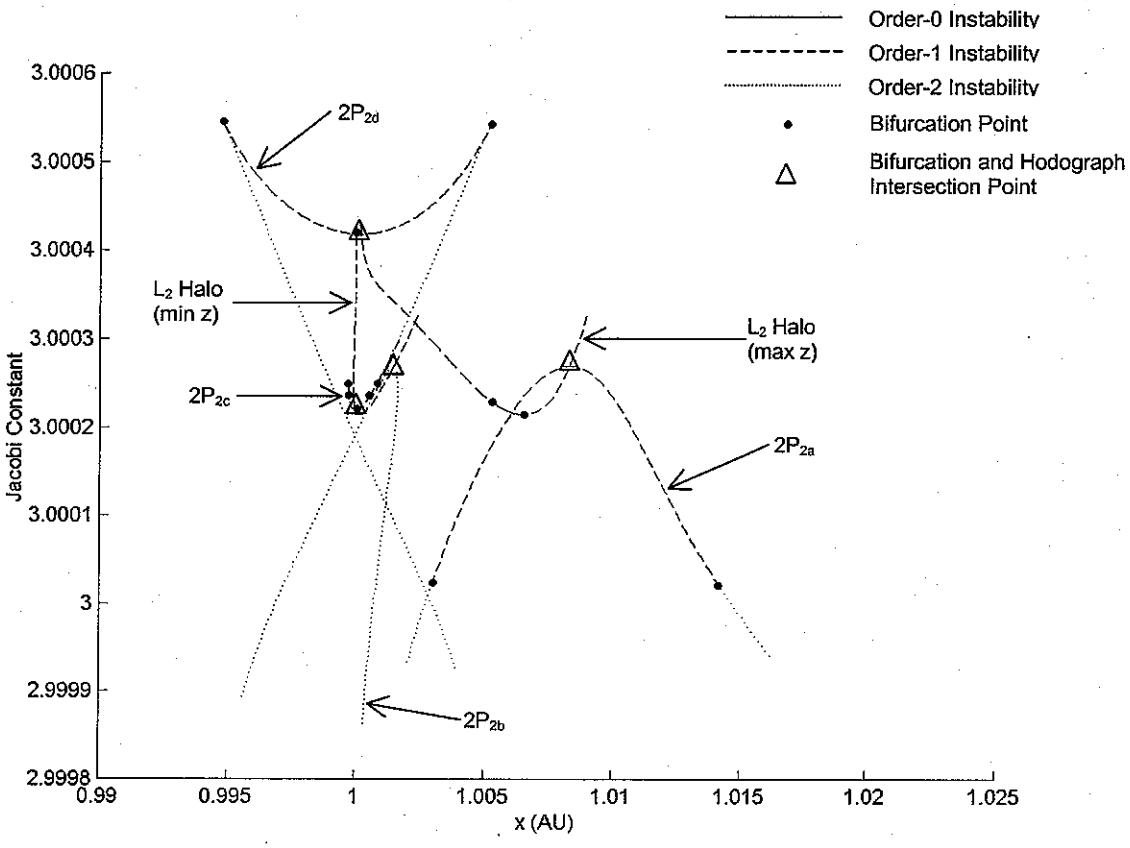

Figure 11 Bifurcation diagram for the L_2 halo, $2P_{2a}$, , $2P_{2b}$, , $2P_{2c}$, , and $2P_{2d}$ families.

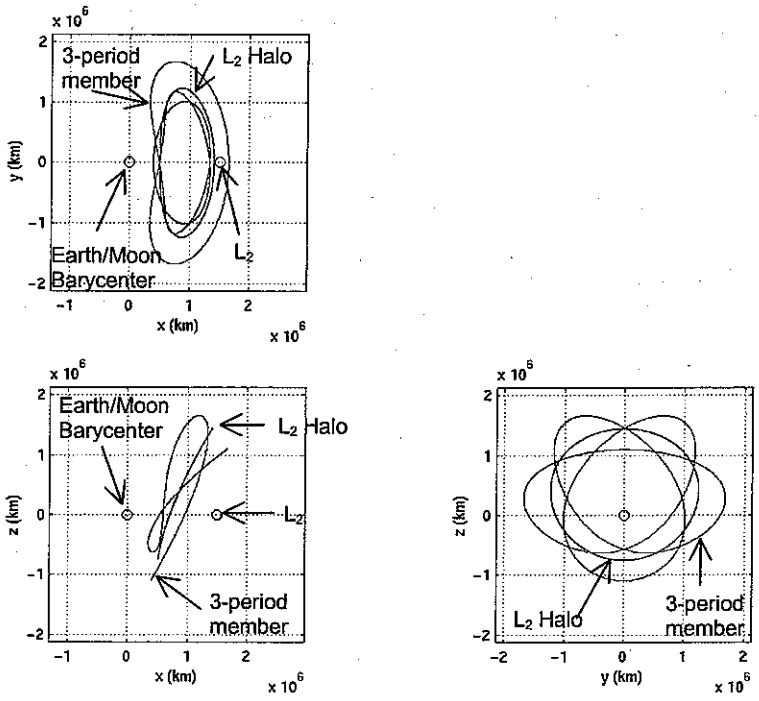

Figure 12 A representative northern 3-period family member and the associated bifurcating northern L_2 family member.

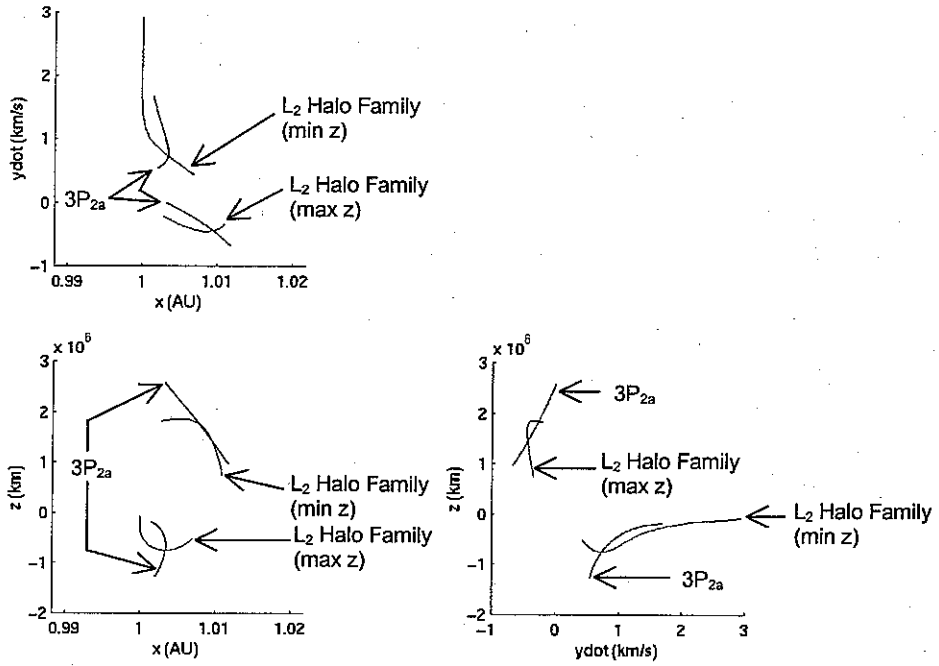

Figure 13 Northern hodographs: planar projections of the L_2 halo and $3P_{2a}$ families.

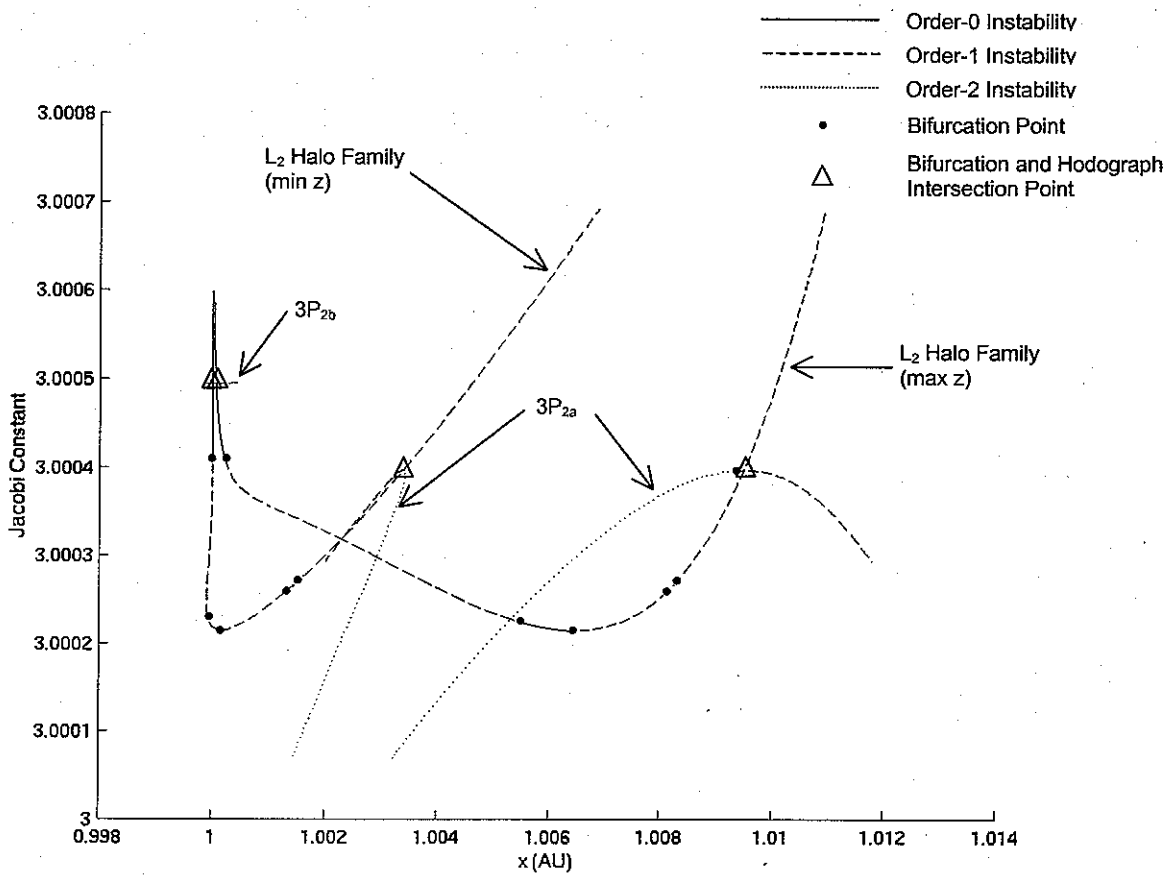

Figure 14 Bifurcation diagram for the L_2 halo, $3P_{2a}$, and $3P_{2b}$ families.

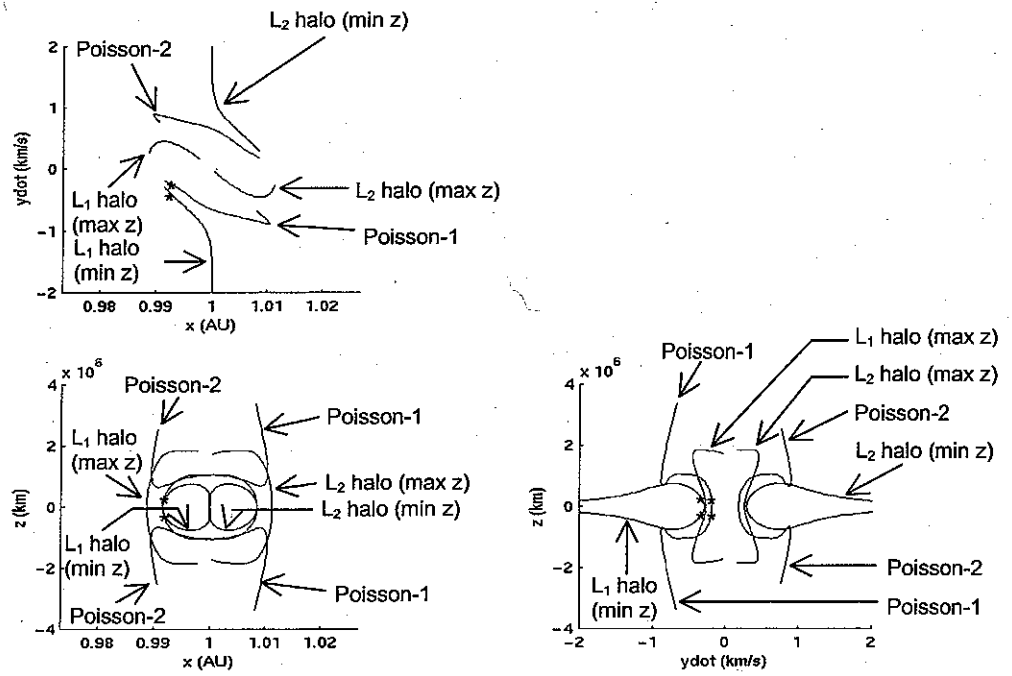

Figure 15 Every hodograph intersection in the xz projection of the northern and southern L_1 and L_2 halo families along with the Poisson-1 and Poisson-2 families, represents a location at which a single impulsive maneuver can be used to shift between families. The other two projections indicate the $\Delta\overline{V}$ necessary to complete the jump.

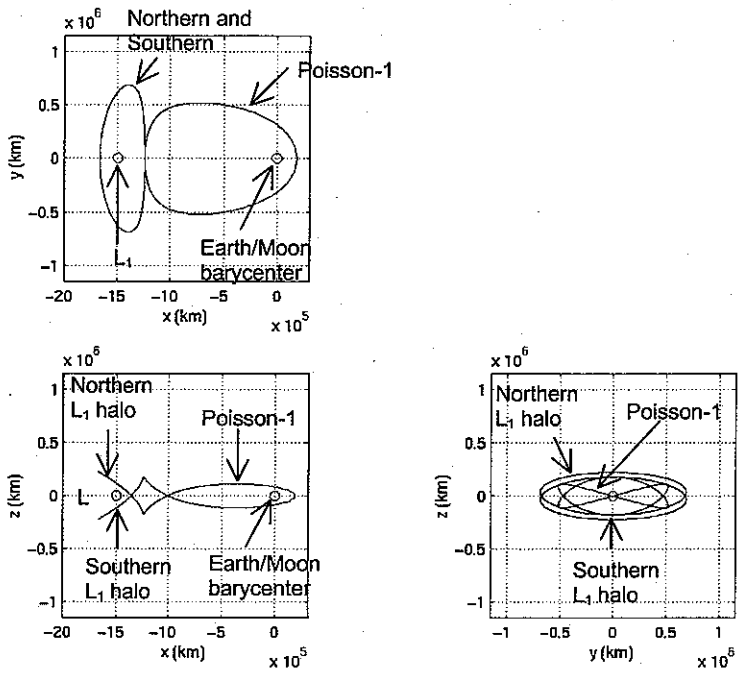

Figure 16 A transfer from a northern L_1 halo to a southern L_1 halo with a two-impulse maneuver via a Poisson-1 family member.

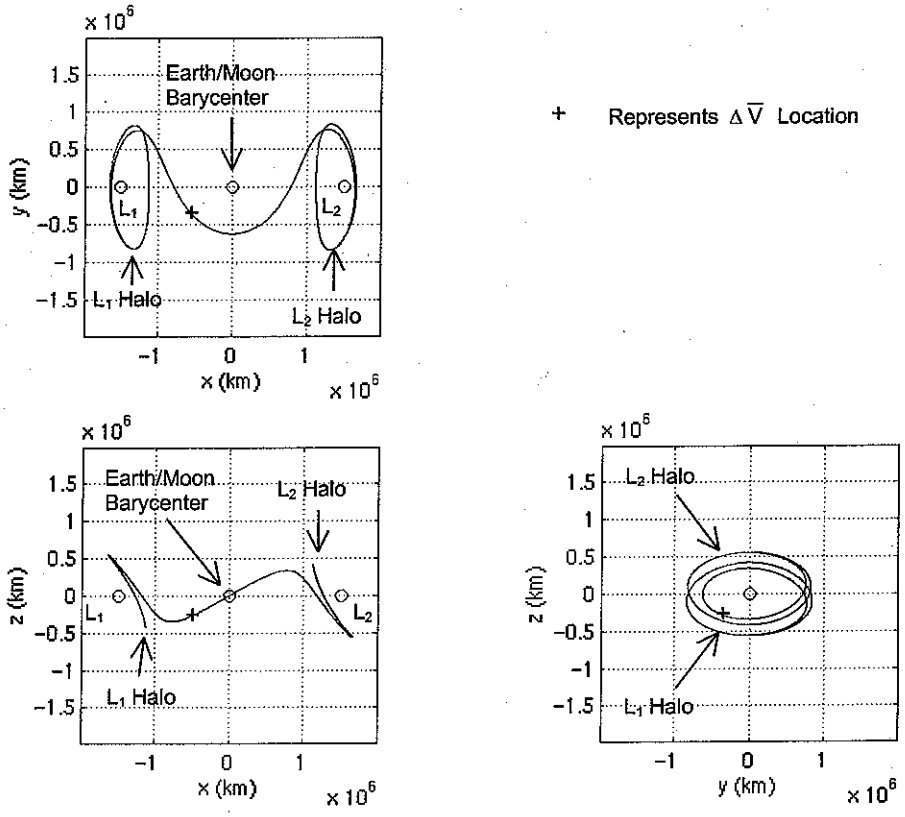

Figure 17 A single impulse (2.39 m/s) creates a transfer from a northern L_1 halo to a southern L_2 halo via intersecting manifolds. The maneuver occurs at the intersection of the unstable L_1 manifold and the stable L_2 manifold.

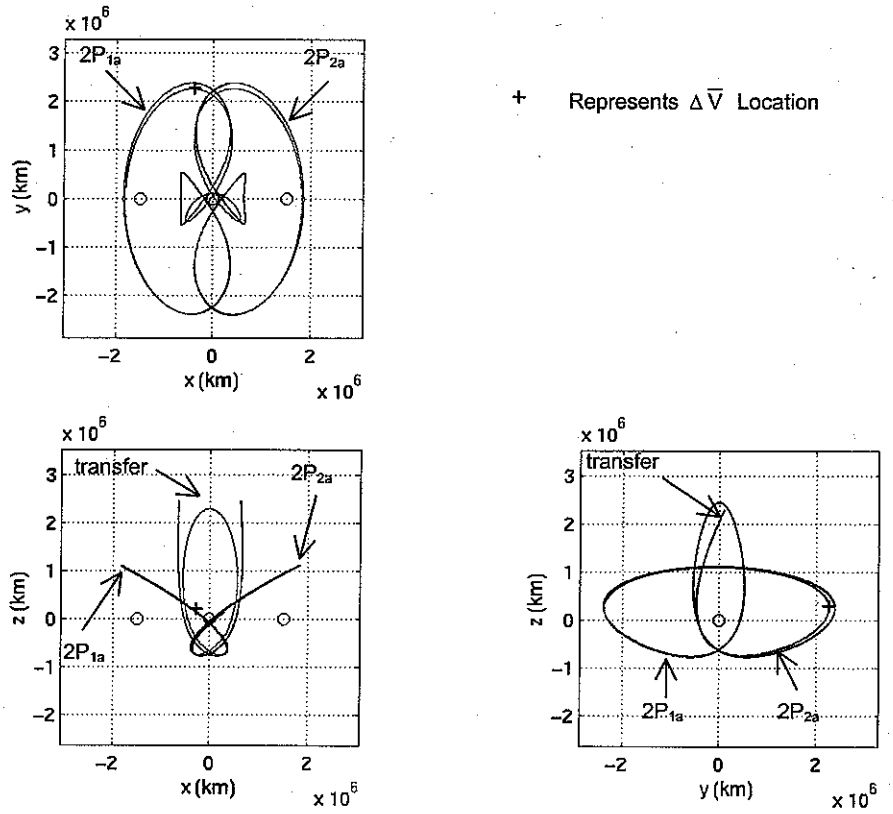

Figure 18 A single maneuver manifold transfer from a northern $2P_{1a}$ to a northern $2P_{2a}$ for a cost of 1.19 m/s.

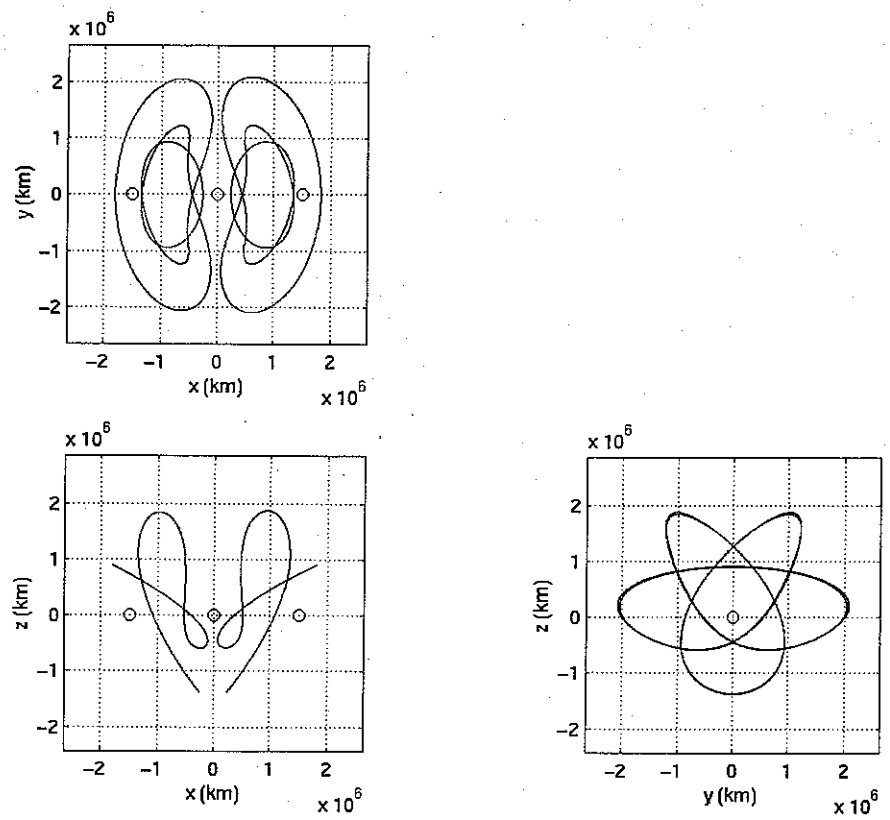

Figure 19 Planar projections of a northern $3P_{1a}$ and a northern $3P_{2a}$ solution.

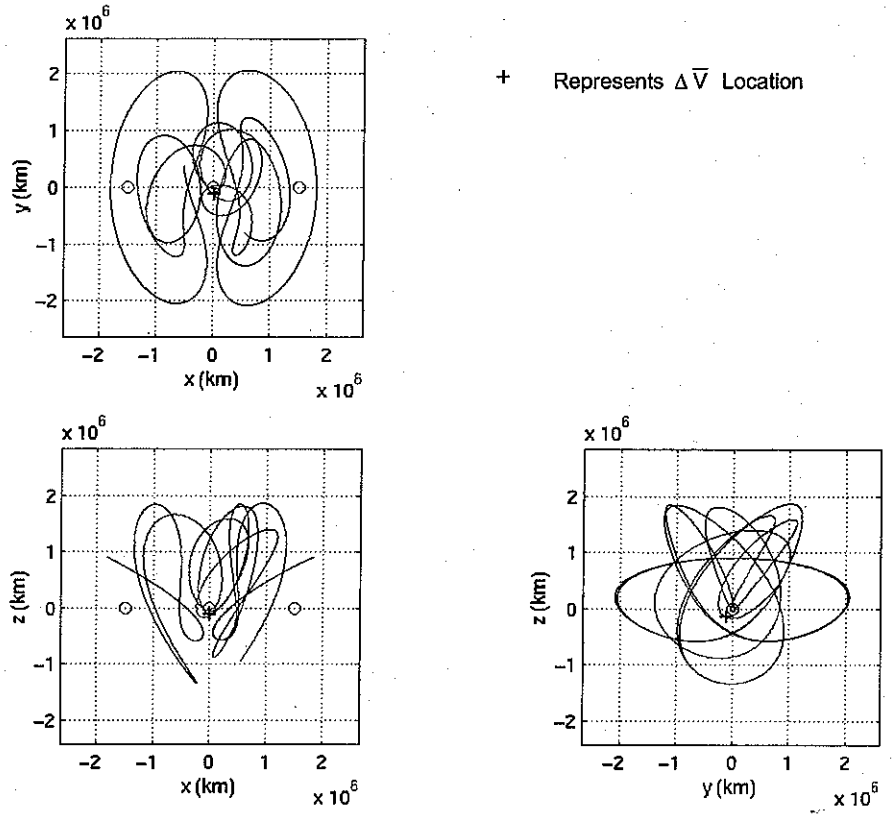

Figure 20 Planar projections of a manifold transfer from the northern $3P_{1a}$ to the northern $3P_{2a}$ particular solutions seen in Figure 19. The transfer cost is 9.1 m/s, while the transfer time is approximately 500 days.